Biosensors and Bioelectronics 26 (2011) 4184–4190

Contents lists available at ScienceDirect

Biosensors and Bioelectronics

journal homepage: www.elsevier.com/locate/bios

Reagentless fluorescent biosensors from artificial families of antigen binding proteins

Frederico F. Miranda[a,b,1], Elodie Brient-Litzler[a,b,1], Nora Zidane[a,b], Frédéric Pecorari[c,d], Hugues Bedouelle[a,b,*]

[a] Institut Pasteur, Department of Infection and Epidemiology, Unit of Molecular Prevention and Therapy of Human Diseases, 25 rue Docteur Roux, 75724 Paris Cedex 15, France
[b] CNRS URA3012, 25 rue Docteur Roux, 75724 Paris Cedex 15, France
[c] CNRS UMR6204, Biotechnology, Biocatalysis and Bioregulation, 2 rue de la Houssinière, BP 92208, 44322 Nantes Cedex 3, France
[d] Université de Nantes, Faculté des Sciences et des Techniques, 2 rue de la Houssinière, BP 92208, 44322 Nantes Cedex 3, France

ARTICLE INFO

Article history:
Received 9 February 2011
Received in revised form 14 April 2011
Accepted 15 April 2011
Available online 22 April 2011

Keywords:
Antibody
Antigen
Binding protein
Biosensor
Fluorescence
Solvatochromic fluorophore

ABSTRACT

Antibodies and artificial families of antigen binding proteins (AgBP) are constituted by a connected set of hypervariable (or randomized) residue positions, supported by a constant polypeptide backbone. The residues that form the binding site for a given antigen, are selected among the hypervariable residues. We showed that it is possible to transform any AgBP of these families into a reagentless fluorescent biosensor, specific of the target antigen, simply by coupling a solvatochromic fluorophore to one of the hypervariable residues that have little or no importance for the interaction with the antigen, after changing this residue into cysteine by mutagenesis. We validated this approach with a DARPin (Designed Ankyrin Repeat Protein) and a Nanofitin (also known as Affitin) with high success rates. Reagentless fluorescent biosensors recognize their antigen in an immediate, quantitative, selective and specific way, without any manipulation of the sample to analyze or addition of reagent.

1. Introduction

Reagentless fluorescent (RF) biosensors can be obtained by integrating a biological receptor, which is directed against the target analyte, and a solvatochromic fluorophore, whose emission properties are sensitive to the nature of its local environment, in a single macromolecule. The fluorophore transduces the recognition event into a measurable optical signal. The use of extrinsic fluorophores, whose emission properties differ widely from those of the intrinsic fluorophores of proteins, tryptophan and tyrosine, enables one to detect and quantify the analyte in complex biological mixtures. The integration of the fluorophore must be done in a site where it is sensitive to the binding of the analyte without perturbing the affinity of the receptor (Altschuh et al., 2006; Loving et al., 2010).

The possibility of obtaining, for any antigen considered as an analyte, RF biosensors which respond to the binding of the antigen by a variation of fluorescence, would have numerous applications in micro- and nano-analytical sciences. Antibodies and artificial families of antigen binding proteins (AgBP) are well suited to provide the recognition module of RF biosensors since they can be directed against any antigen. A general approach to integrate a solvatochromic fluorophore in an AgBP when the atomic structure of the complex with its antigen is known, and thus transform it into a RF biosensor, has been described recently (Brient-Litzler et al., 2010). A residue of the AgBP is identified in the neighborhood of the antigen in their complex. This residue is changed into a cysteine by site-directed mutagenesis. The fluorophore is chemically coupled to the mutant cysteine. When the design is successful, the coupled fluorophore does not prevent the binding of the antigen, this binding shields the fluorophore from the solvent, and it can be detected by a change of fluorescence.

The variable fragments (Fv) of antibodies comprise a polypeptide backbone, which is conserved both in sequence and structure, and six loops of hypervariable residues, which are grafted onto the backbone and form the antigen binding site (paratope). The artificial families of AgBPs are similarly constructed. For example, one may start from a natural family of binding proteins and either design a canonical polypeptide backbone or select a representative member from this family (Binz et al., 2003; Drevelle et al., 2009; Famm et al., 2008; Mouratou et al., 2007; Urvoas et al., 2010). The residue positions that contribute to antigen binding in the various elements of the natural family, are identified through a careful anal-

* Corresponding author at: Institut Pasteur, CNRS URA3012, 25 rue Docteur Roux, 75724 Paris Cedex 15, France. Tel.: +33 1 45688379; fax: +33 1 40613533.
E-mail address: hugues.bedouelle@pasteur.fr (H. Bedouelle).
[1] These authors contributed equally to this work.

0956-5663/$ – see front matter © 2011 Elsevier B.V. All rights reserved.
doi:10.1016/j.bios.2011.04.030

ysis of the available structural and functional data (Arcus, 2002; Mosavi et al., 2002; Theobald et al., 2003). Generally, these positions form a connected set on one side of the canonical protein. The corresponding residues are then randomized at the genetic level to constitute a random library of genes, coding for an artificial family of AgBPs. We refer to the positions of the randomized residues as hypervariable, by analogy with antibodies. The elements of a random family that bind a target antigen, are selected in vivo or in vitro by methods of display that physically link a gene and its product, e.g. phage, ribosome or yeast display (Beste et al., 1999; Binz et al., 2004; Heyd et al., 2003; Jespers et al., 2004; Mouratou et al., 2007; Nord et al., 1997).

The methods for the selection of AgBPs from artificial families imply that the residues that form structural or energetic contacts with the antigen, are mainly located at hypervariable positions. Antibodies and AgBPs generally use only a subset of the residues at the hypervariable positions to bind their target antigen and the hypervariable positions that are not used to form contacts with the antigen, are located in its neighborhood (MacCallum et al., 1996).

Here, we explored the possibility of deriving RF biosensors from any element of artificial families of AgBPs, in the absence of specific structural data, by using their peculiar method of construction. Our strategy consisted in individually changing the residues of the hypervariable positions into cysteine at the genetic level, in chemically coupling a solvatochromic fluorophore with the mutant cysteine, and then in ordering the resulting conjugates through their relative sensitivity s_r, that involves both their affinity for the antigen and their relative variation of fluorescence signal. To validate this approach, we used two different AgBPs, for which no specific structural data is available: H4S, a Nanofitin (also known as Affitin) which is directed against hen egg-white lysozyme (HEL) (Cinier et al., 2009; Pecorari and Alzari, 2008), and MBP3_16, a DARPin which is directed against the MalE protein from *Escherichia coli* (Binz et al., 2004).

2. Materials and methods

2.1. Buffers and genetic constructions

Buffer A was 500 mM NaCl, 50 mM Tris–HCl, pH 8.0; buffer B, as buffer A but pH 7.5; buffer C, 150 mM NaCl, 50 mM Tris–HCl, pH 7.4; buffer D, 0.005% (v/v) Tween 20, 0.1 mg/mL BSA in buffer C; buffer E, 5 mM dithiothreitol (DTT) in buffer D; buffer F, 0.005% (v/v) Tween 20 and 5 mM DTT in buffer C.

The *E. coli* strains NEB-Express-I^q (New England Biolabs), XL1-Blue (Bullock et al., 1987) and AVB99 (Smith et al., 1998) have been described. Plasmid pH4S codes for H4S, a Nanofitin which is directed against hen egg-white lysozyme (HEL) (Cinier et al., 2009). The sequence of H4S is identical to that previously published, except that residue Cys29 has been changed into Ser29 (Pecorari and Alzari, 2008). The numbering does not take an engineered extension NH2-MRGSHHHHHHG into account (Fig. S1 in Appendix A). Plasmid pQEMBP3_16 codes for MBP3_16, a DARPin which is directed against MalE (GenBank AY326426) (Binz et al., 2004). All the recombinant proteins carried a hexahistidine tag (H6). Changes of residues were introduced by mutagenesis of the expression plasmids as described (Brient-Litzler et al., 2010).

2.2. Production and characterization of proteins and conjugates

The parental protein H4S(wt) and its mutant derivatives were produced in the cytoplasm of the recombinant strain NEB-Express-I^q(pH4S) and derivatives. The MalE protein was produced in the cytoplasm of XL1-Blue(pQEMBP), bt-MalE in AVB99(pAT224) and MBP3_16 and its mutant derivatives in XL1-Blue(pQEMBP3_16) and derivatives as described (Binz et al., 2004). The proteins were purified by affinity chromatography on a column of fast flow Ni-NTA resin (Qiagen) and eluted with imidazole, in buffer A or B according to their pI value. The analysis of the purification fractions by SDS-PAGE in the presence or absence of 2.5% (v/v, 0.4 M) 2-mercaptoethanol, the quantification of the protein bands, and the measurement of the protein concentrations by absorbance spectrometry were performed as described (Brient-Litzler et al., 2010). The pure fractions (>98% homogeneous in reducing conditions), were pooled and kept at −80 °C. The conjugates between N-((2-(iodoacetoxy)ethyl)-N-methyl)amino-7-nitrobenz-2-oxa-1,3-diazole (IANBD ester; Invitrogen) and the cysteine mutants of either H4S or MBP3_16 were prepared essentially as described (Section S1 in Appendix A) (Brient-Litzler et al., 2010). The conjugate between 2-mercaptoethanol and the IANBD ester was prepared by mixing the two molecules in stoechiometric amounts and then incubating the mixture for 30 min at 25 °C. In the following paragraphs, all the characterizations of proteins and conjugates were performed at 25 °C. In addition, those of the cysteine mutants were performed in the presence of 5 mM DTT to reduce any intermolecular disulfide bond.

2.3. Fluorescence variation and antigen binding: theory

A conjugate (or biosensor) B and antigen A form a 1:1 complex B:A, with a dissociation constant K_d, according to the reaction:

$$B + A \leftrightarrow B:A \tag{1}$$

The total concentration $[B]_0$ was kept constant and the total concentration $[A]_0$ was varied in titration experiments. The fluorescence intensity F of the conjugate at a given value of $[A]_0$ satisfies the following equation:

$$\frac{(F - F_0)}{F_0} = \frac{\Delta F}{F_0} = \left(\frac{\Delta F_\infty}{F_0}\right)\left(\frac{[B:A]}{[B]_0}\right) \tag{2}$$

where F_0 and F_∞ are the values of F at zero and saturating concentrations of A, $\Delta F = (F - F_0)$ and $\Delta F_\infty = (F_\infty - F_0)$ (Renard et al., 2003). The values of $\Delta F_\infty/F_0$ and K_d were determined by fitting Eq. (2), in which [B:A] is deduced from the equations of equilibrium and mass conservation, to the experimental values of $\Delta F/F_0$, measured in a titration experiment as described (Eq. (S4) in Appendix A) (Brient-Litzler et al., 2010; Renard et al., 2003).

The sensitivity s and relative sensitivity s_r of a conjugate can be defined by the following equations for the low values of $[A]_0$, i.e. in the initial part of the titration curve:

$$\Delta F = s[A]_0 \tag{3}$$

$$\frac{\Delta F}{F_0} = \frac{s_r[A]_0}{[B]_0} \tag{4}$$

s and s_r can be expressed as functions of characteristic parameters of the conjugate:

$$s_r = \left(\frac{\Delta F_\infty}{F_0}\right)\left(\frac{[B]_0}{(K_d + [B]_0)}\right) \tag{5}$$

$$s = f_b s_r \tag{6}$$

where $f_b = F_0/[B]_0$ is the molar fluorescence of the free conjugate (Renard and Bedouelle, 2004). The lower limit of detection $\delta[A]_0$ of the conjugate is linked to the lower limit of measurement of the spectrofluorometer δF by the following equations:

$$\delta[A]_0 = s^{-1}\delta F = s_r^{-1}[B]_0\left(\frac{\delta F}{F_0}\right) \tag{7}$$

2.4. Fluorescence variation and antigen binding: measurements

We treated the binding and fluorescence experiments at equilibrium as if the preparations of conjugates were homogeneous. The binding reactions were conducted by incubating the conjugate and antigen (HEL, MalE or BSA) for a fixed duration t, in a volume of 1 mL with gentle shaking in the dark. We used $[B]_0 = 0.3\ \mu M$ and $t = 30$ min for the H4S conjugates; $[B]_0 = 1.0\ \mu M$ and $t = 60$ min for the MBP3_16 conjugates. The reactions were carried out in buffer C or in a mixture v:$(1-v)$ of calf serum and buffer C. The fluorescence of the IANBD conjugates was excited at 485 nm and its intensity measured between 520 and 550 nm with a FP-6300 spectrofluorometer (Jasco). The slit widths of excitation and emission were respectively equal to 5 nm and 20 nm for the H4S conjugates, and to 2.5 nm and 5 nm for the MBP3_16 conjugates. The signal of the antigen alone was measured in an independent experiment and subtracted from the global signal of the binding mixture to give the specific fluorescence intensity F of each conjugate. The experiments of fluorescence quenching by potassium iodide KI were performed in buffer C, essentially as described (Brient-Litzler et al., 2010).

2.5. Affinity in solution as determined by competition Biacore

The affinities in solution were determined essentially as described (Brient-Litzler et al., 2010). The binding reactions between H4S(wt) and HEL (250 μL) were conducted by incubating 20 nM of H4S(wt) with variable concentrations of HEL for 30 min in buffer D. The binding reactions between the MBP3_16 derivatives and MalE (100 μL) were conducted by incubating a fixed concentration of MBP3_16 molecules with variable concentrations of MalE in buffer F for > 1 h. The wild type MBP3_16(wt) and its mutant derivatives were used at a concentration of 50 nM, except those carrying mutations T79C, D81C and W90C, which were used at 500 nM to obtain a sufficient signal. The concentration of the free molecules of either H4S or MBP3_16 derivative was then measured by surface plasmon resonance with a Biacore 2000 instrument (Section S1).

2.6. R_{eq} measurement by Biacore

The Biacore experiments were performed at a flow rate of 25 μL min^{-1} with streptavidin SA sensor chips (Biacore Life Sciences). A first cell of the sensor chip was used as a reference, i.e. no ligand was immobilized on the corresponding surface. A second cell was loaded with a high density of the bt-MalE protein (>2000 Resonance Units, RU). The MBP3_16 derivatives, at a concentration $C = 50$ nM in buffer F, were injected for 6 min to monitor association. The chip surface was regenerated between the runs by injection of 10 mM glycine–HCl, pH 3.0, for 24 s. The experimental data were cleaned up with the Scrubber program (Biologic Software) and analyzed with the Biaevaluation 4.1 program (Biacore Life Sciences) to determine R_{eq}, the resonance signal at equilibrium. R_{eq}, is related to the dissociation constant K_d by equation (Nieba et al., 1996):

$$R_{eq} = \frac{R_{max} C}{(C + K_d)} \quad (8)$$

Two independent measurements were performed for each MBP3_16 derivative.

3. Results

3.1. Production and oligomeric state of cysteine mutants

Several artificial families of AgBPs have been developed recently. They are devoid of cysteine residue and have favorable properties of recombinant expression in *E. coli*, solubility and stability, contrary to recombinant antibodies. The Nanofitins are derived from the Sac7d protein of *Sulfolobus acidocaldarius*, which has an oligonucleotide/oligosaccharide binding (OB) fold, and they comprise 14 randomized positions. Two additional positions, 28 and 39, are not randomized although the residues at the corresponding positions form contacts between some OB-fold proteins and their cognate partners (Fig. S1 in Appendix A) (Pecorari and Alzari, 2008). The residues at the 14 randomized positions of the Nanofitin H4S, directed against hen egg-white lysozyme (HEL), and at its positions Lys28 and Lys39 were changed individually into cysteine by site-directed mutagenesis of the coding gene.

The Designed Ankyrin Repeat Proteins (DARPins) constitute a well characterized family of AgBP. The ankyrin modules are present in thousands of natural proteins and involved in recognitions between proteins (Li et al., 2006; Mosavi et al., 2004). Consensus sequences of the ankyrin modules have been established and combinatorial libraries of DARPins generated by randomization of the residues that potentially belong to the antigen binding site, and by assemblage of a few ankyrin modules between defined N- and C-terminal modules (Binz et al., 2003). The DARPin MBP3_16 comprises two ankyrin modules and is directed against the MalE protein of *E. coli* (Binz et al., 2004). The residues at the 12 fully randomized positions of MBP3_16 were changed individually into cysteine while the residues at positions 69 and 102, which are only partially randomized, were neglected (Fig. S2).

The parental proteins, H4S(wt) and MBP3_16(wt), and their mutant derivatives were produced in the cytoplasm of *E. coli* and purified through their hexahistidine tag to >95% homogeneity. The yields of purified protein varied between 4 and 46 mg/L of culture in flask for the H4S derivatives and between 30 and 100 mg/mL for the MBP3_16 derivatives. For some mutant proteins, we observed that a small proportion of the polypeptide molecules were engaged in an intermolecular disulfide bond, through their mutant cysteine residue (Table S1 in Appendix A).

3.2. Conjugation and its yield

We submitted the purified preparations of the mutant proteins to a reaction of reduction before coupling with the thiol reactive fluorophore N-((2-(iodoacetoxy)ethyl)-N-methyl)amino-7-nitrobenz-2-oxa-1,3-diazole (IANBD ester), to break open the potential intermolecular disulfide bonds and ensure that the mutant cysteine residue would be in a reactive state. The products of the coupling reaction were separated from the unreacted fluorophore by chromatography on a nickel ion column. The coupling yield y_c, defined as the number of fluorophore groups per protein molecule, was calculated from the absorbance spectra of the purified reaction product ($72 \pm 3\%$ for the H4S conjugates; $97 \pm 1\%$ for the MBP3_16 conjugates; mean ± SE). The synthesis yield y_s of the coupling procedure, i.e. the proportion of protein molecules that remained at the end of the procedure, was similar and high for all the conjugates ($65 \pm 3\%$ for the H4S conjugates and $71 \pm 2\%$ for the MBP3_16 conjugates).

Table 1
Properties of H4S conjugates, as derived from fluorescence experiments.

Residue	y_c	λ_{max} (nm)	f_b (FU μM^{-1})	$\Delta F_\infty/F_0$	K_d (nM)	s_r
Phe7	0.86	539.0	1760	0.26 ± 0.01	42 ± 13	0.22
Trp8	0.72	536.5	427	1.47 ± 0.04	189 ± 50	0.90
Asn9	0.43	539.0	232	0.52 ± 0.01	7 ± 2	0.50
Val21	0.87	537.0	531	6.30 ± 0.04	296 ± 19	3.17
Trp22	0.77	529.5	4375	0.3 ± 0.1	1226 ± 1141	0.06
Lys24	0.68	536.0	433	8.8 ± 0.1	98 ± 17	6.61
Ala26	0.54	539.0	664	7.9 ± 0.1	206 ± 27	4.66
Lys28	0.75	537.5	1888	0.26 ± 0.01	28 ± 8	0.24
Ser29	0.73	538.5	1428	0.55 ± 0.01	33 ± 6	0.50
Leu31	0.80	538.0	193	4.9 ± 0.4	8356 ± 2754	0.17
Ile33	0.90	537.5	191	*nm*	*nm*	nm
Lys39	0.68	538.5	764	1.65 ± 0.02	126 ± 14	1.16
Asn40	0.65	537.5	458	0.57 ± 0.05	2004 ± 894	0.07
Tyr42	0.69	537.5	286	6.6 ± 0.2	2479 ± 487	0.72
Asp44	0.70	537.0	689	1.50 ± 0.04	623 ± 106	0.49
Thr46	0.85	538.5	1922	0.36 ± 0.01	100 ± 32	0.27

Column 1, residue with which the fluorophore was coupled. y_c, number of molecules of fluorophore per molecule of H4S in a purified preparation of the conjugate (coupling yield); λ_{max}, wavelength of the maximal value of F_0; f_b, molar fluorescence of the free conjugate at λ_{max}, calculated with a concentration of conjugate equal to $y_c[B]_0$; $\Delta F_\infty/F_0$, maximal variation of F at λ_{max}; s_r, relative sensitivity of the conjugate at a total concentration $[B]_0 = 0.3$ μM; nm, not measurable. The entries for $\Delta F_\infty/F_0$ and K_d give the value and associated SE from the fitting of Eq. (2) to the data points in the titration experiments. The fluorescence experiments were performed at 25 °C in buffer C. The experiments for Trp8, Val21, Lys24, Ala26, Ser29, Leu31 and Lys39 were performed in duplicate with identical results. The Pearson parameter in the fittings was $R > 0.992$ except for Phe7 ($R = 0.98$) and Trp22 ($R = 0.72$). The K_d value for H4S(wt) was equal to 40.3 ± 1.6 nM, as measured by competition Biacore at 25 °C in buffer D (value ± SE in curve fit; see Section 2.5).

3.3. Fluorescence properties of the H4S conjugates

The free H4S conjugates were excited at 485 nm and their emission spectra were recorded. The maximum of fluorescence intensity had a wavelength λ_{max} that varied slightly between conjugates and ranged from 529.5 to 540 nm. The experiments of spectrofluorometry with the H4S conjugates were performed at their λ_{max} value thus determined and at a total concentration of conjugate $[B]_0 = 0.3$ μM. The fluorescence intensities F_0 of the free conjugates were comprised between 37 and 1921 FU (arbitrary fluorescence units) at this concentration and corresponded to molar fluorescences f_b between 191 and 4375 FU μM^{-1} (Table 1).

We tested the responsiveness of the H4S conjugates to the binding of their HEL antigen by measuring the relative variation $\Delta F/F_0 = (F - F_0)/F_0$ in their fluorescence intensity F between their HEL-bound and free states. Titrations of the conjugates were performed with ≥17 different concentrations of antigen (Fig. 1). The dissociation constant K_d and maximal variation $\Delta F_\infty/F_0$ were deduced by fitting Eq. (2), which links $\Delta F/F_0$ and the total concentration of antigen $[A]_0$, to the experimental data points (Section 2.3). The values of K_d varied widely between conjugates, between 7 nM and 8 μM. The value of $\Delta F_\infty/F_0$ was >0.5 for 11 of the conjugates, i.e. F increased by >1.5-fold on HEL binding (Table 1).

3.4. Ranking of the H4S conjugates

The conjugates gave a wide range of values for $\Delta F_\infty/F_0$ and K_d. We classified them according to their relative sensitivity s_r. This parameter relates the relative variation $\Delta F/F_0$ of the fluorescence signal to the relative concentration $[A]_0/[B]_0$ of antigen for the low values of the latter, where $[A]_0$ and $[B]_0$ are the total concentrations of antigen and conjugate, respectively, in the titration reaction (Eq. (4); $[A]_0/[B]_0$ can be viewed as the concentration of antigen, normalized to the concentration of conjugate). s_r is an intrinsic dimensionless parameter. Its value does not depend on the spectrofluorometer or its set up, and should remain constant between experiments, instruments and laboratories. The value of s_r depends on the values of $[B]_0$ and K_d according to a Michaelis–Menton law and its maximal value is equal to $\Delta F_\infty/F_0$ (Eq. (5)). The lower limit of detection of a conjugate can then be deduced from that of the spectrofluorometer, knowing its total concentration $[B]_0$, value of s_r and molar fluorescence f_b (Eq. (7)).

We calculated the variation of s_r for each H4S conjugate as a function of $[B]_0$ from its K_d and $\Delta F_\infty/F_0$ values (Fig. 2). These variations showed that the classification of the conjugates according to their values of s_r could vary as a function of $[B]_0$. For $[B]_0 \leq 0.45$ μM, the coupling positions ranked in the following decreasing order, i.e. starting with the highest sensitivity s_r: Lys24 > Ala26 > Val21 > Lys39 > Trp8 > Tyr42 (Table 1 and Fig. 2). The conjugate at position Lys24, H4S(K24ANBD), had a value $s_r = 6.6$ when used at a concentration $[B]_0 = 0.3$ μM, and a lower limit of detection $\delta[A]_0 = 0.68$ nM since our spectrofluorometer could detect a relative variation of fluorescence $\delta F/F_0 = 1.5\%$ in our experimental conditions. This s_r value meant that the fluorescence signal

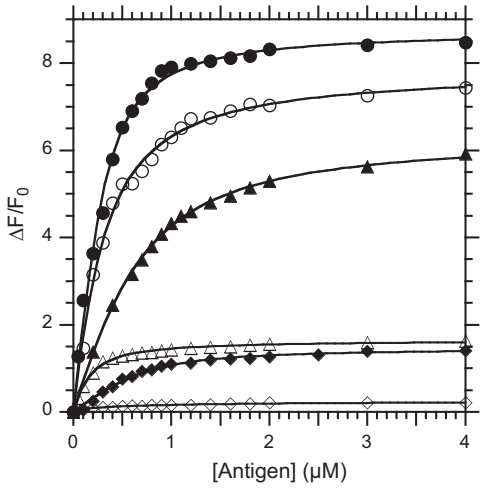

Fig. 1. Titration of H4S conjugates, monitored by fluorescence. The experiments were performed at 25 °C in buffer C. The total concentration of H4S conjugate, measured by A_{280}, was equal to 0.3 μM. The total concentration in cognate (HEL) or non-cognate (BSA) antigen is given along the x axis; data points at 8.0 μM are not shown in the figure. The continuous curves correspond to the fitting of Eq. (2) to the experimental values of $\Delta F/F_0$ (Section 2.3). HEL as antigen: closed diamonds, fluorophore at position Trp8; closed triangles, Val21; closed circles, Lys24; open circles, Ala26; open triangles, Lys39. BSA as antigen: open diamonds, Lys24.

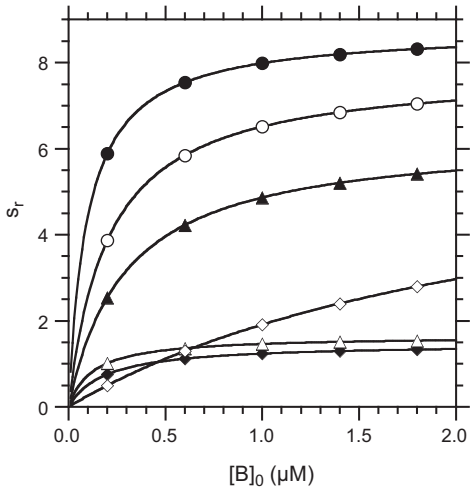

Fig. 2. Relative sensitivities s_r of the H4S conjugates at 25 °C in buffer C as a function of their concentration. This figure is a plot of Eq. (5), using the parameters listed in Table 1. The s_r parameter relates the relative variation of fluorescence intensity $\Delta F/F_0$ and the relative concentration of antigen $[A]_0/[B]_0$ for the low values of $[A]_0$, where $[A]_0$ and $[B]_0$ are the total concentrations of antigen and conjugate in the binding reaction, respectively (Eq. (4)). Closed diamonds, fluorophore at position Trp8; closed triangles, Val21; closed circles, Lys24; open circles, Ala26; open triangles, Lys39; open diamonds, Tyr42.

F increased 6.6-fold faster than the occupancy of the conjugate by its antigen, both in relative terms, for low concentrations of HEL.

3.5. Specificity, selectivity and mechanism of signal variation

We further characterized the H4S(K24ANBD) conjugate. To test its specificity of recognition, we compared its titrations with HEL and bovine serum albumin (BSA). H4S(K24ANBD) weakly bound BSA with values of K_d much higher and values of $\Delta F_\infty/F_0$ much lower than for HEL: $K_d = 1.0 \pm 0.3$ μM and $\Delta F_\infty/F_0 = 0.26 \pm 0.01$ (Fig. 1). As a result, the sensitivity s_r of H4S(K24ANBD) was 106-fold lower for BSA than for HEL. Therefore, the variation of the $\Delta F/F_0$ signal was indeed specific for HEL, the cognate antigen.

The selectivity of a biosensor refers to its recognition of a particular analyte in a complex mixture without interference from other components (Vessman et al., 2001). We characterized the selectivity of the H4S(K24ANBD) conjugate by comparing its fluorescence properties in serum and in a defined buffer. As a control, we used a conjugate between IANBD and 2-mercaptoethanol. We observed that the fluorescence response of the H4S conjugate was lower in serum than in buffer, due to the absorbance of light by the serum, and that some molecules of the serum interacted with the 2-mercaptoethanol conjugate. However, H4S(K24ANBD) was operational in ≤50% serum (see Section S2 of Appendix A).

The fluorescence of the H4S(K24ANBD) conjugate was quenched by potassium iodide (KI), both in its free and HEL-bound states. The quenching varied linearly with the concentration of KI. The corresponding value of the Stern–Volmer constant was higher for the free state of the conjugate than for its HEL-bound state: $K_{SV} = 6.7 \pm 0.1\ M^{-1}$ versus $2.5 \pm 0.1\ M^{-1}$. These results showed that the fluorescence increase was due to a shielding of the fluorescent group from the solvent by the binding of the antigen (Fig. S4; see Section S2 of Appendix A for details).

3.6. Affinities of H4S(wt) and its conjugates

The dissociation constants K_d in solution between the H4S conjugates and HEL were determined by titrations, monitored with fluorescence (Fig. 1). This method was not applicable to the parental protein H4S(wt). We therefore determined its K_d value in solution by experiments of competition Biacore and found that it was equal to 40.3 ± 1.6 nM (Section 2.5). Comparison of the K_d values for H4S(wt) and its conjugates, all of them determined in solution, showed that the conjugates could be distributed in three subsets, according to their K_d values: subset R1, composed of the six conjugates whose K_ds were strongly increased, by >15-fold, relative to H4S(wt); subset R2, the six conjugates whose K_ds were weakly increased, by <7.5-fold; and subset R3, the four conjugates whose K_ds were unaffected or even improved. Additional experiments showed that the increase in K_d could result from the change of the target residue into Cys or from the coupling of the fluorophore (Section S2).

Table 2
Properties of Cys mutants of MBP3_16.

Mutation	R_{eq} (RU)	K_d (nM)	$\Delta\Delta G$ (kcal mol^{-1})
WT	400 ± 2	43.2 ± 0.4	0.00 ± 0.01
M43C	354 ± 3	32 ± 2	−0.17 ± 0.03
N45C	364 ± 1	27 ± 4	−0.27 ± 0.09
F46C	8 ± 1	>1000	>2
V48C	264 ± 3	73 ± 7	0.31 ± 0.06
Y56C	4.2 ± 0.1	>1000	>2
W57C	5.3 ± 0.2	>1000	>2
S76C	468 ± 4	19 ± 4	−0.5 ± 0.1
A78C	313 ± 2	31 ± 2	−0.19 ± 0.03
T79C	56 ± 1	257 ± 9	1.06 ± 0.02
D81C	53 ± 1	290 ± 59	1.1 ± 0.1
K89C	239 ± 1	60 ± 4	0.20 ± 0.04
W90C	25 ± 1	972 ± 185	1.8 ± 0.1

The experiments were performed at 25 °C in buffer F. WT, parental MBP3_16 protein; R_{eq}, Biacore signal at steady state for the binding of the DARPin to immobilized bt-MalE; K_d, dissociation constant between the DARPin and MalE, as measured in solution by competition Biacore; $\Delta G = -RT \ln K_d$, free energy of interaction between the MBP3_16 mutant and MalE; $\Delta\Delta G$, variation of ΔG resulting from the mutation. The mean value and SE are given for R_{eq} in two independent experiments; for the K_d of the parental DARPin in four independent experiments; for the K_ds of the mutant DARPins in the fitting of the equilibrium equation to the experimental data; and for $\Delta\Delta G$ as deduced from SE on the K_d values (Eqs. (S8) and (S9)).

3.7. Cysteine scanning of the randomized positions in MBP3_16

The above and previous results suggested to avoid the residues whose change into Cys strongly increases K_d since the coupling of a fluorescent group exceptionally reverts the deleterious effect of such a mutation. For MBP3_16, we therefore chose first to identify the changes of the randomized positions into Cys that decreased its affinity for the MalE protein and then to restrict the construction and characterization of conjugates to the other randomized positions.

We characterized the properties of recognition between the Cys mutants of MBP3_16 and MalE by two methods, using the Biacore instrument. This characterization was performed in the presence of dithiothreitol (5 mM) to eliminate intermolecular disulfide bonds. In a preliminary experiment, we immobilized a biotinylated form of MalE (bt-MalE), on a streptavidin sensor chip, injected each of MBP3_16(wt) and its mutant derivatives onto the chip at a fixed concentration (50 nM) in the liquid phase, and measured the variation of resonance signal at equilibrium R_{eq}. The R_{eq} value for MBP3_16(wt) was equal to 400 ± 2 RU (Resonance Units). The four mutations that changed aromatic residues, F46C, Y56C, W57C and W90C, decreased the value of R_{eq} below 25 RU. The other mutations affected R_{eq} to varying extent, with values comprised between 53 and 468 RU (Table 2).

Except for the mutants at positions 46, 56 and 57, the R_{eq} values were large enough to allow the determination of the dissociation constant K_d between the mutant DARPins and MalE by experiments of competition Biacore in solution (Table 2; Fig. S5). The K_d value for MBP3_16(wt) was equal to 43.2 ± 0.4 nM. Six mutations changed K_d

Table 3
Properties of MBP3_16 conjugates, as derived from fluorescence experiments.

Residue	y_c	λ_{max} (nm)	f_b (FU μM^{-1})	$\Delta F_\infty/F_0$	K_d (nM)	s_r
Met43	1.13	540	37.9 ± 0.5	0.46 ± 0.01	153 ± 38	0.40
Asn45	1.03	539	23.5 ± 0.1	1.69 ± 0.03	248 ± 35	1.35
Ser76	1.02	538	32.8 ± 0.1	0.65 ± 0.01	79 ± 16	0.61
Ala78	0.58	538	27.0 ± 0.3	1.00 ± 0.03	146 ± 35	0.83
Lys89	1.05	535	6.5 ± 0.1	5.8 ± 0.1	687 ± 57	3.46

The experiments were performed at 25 °C in buffer C. See the legend of Table 1 for the definition of the parameters. s_r, relative sensitivity of the conjugate at a total concentration $[B]_0 = 1.0$ μM.

by less than 2-fold; two mutations, T79C and D81C, increased K_d by 6-fold; four mutations, changing aromatic residues and listed above, increased K_d by more than 20-fold. We observed that the values of R_{eq} and K_d were non-linearly correlated. Thus, R_{eq} could be a useful approximation of K_d (Fig. S6).

3.8. Fluorescence properties and ranking of MBP3_16 conjugates

We studied the conjugates of the five best Cys mutants, i.e. those whose K_d values were lower than 60 nM and which corresponded to positions Met43, Asn45, Ser76, Ala78 and Lys89. As described above for the H4S conjugates, the free MBP3_16 conjugates were excited at 485 nm and their emission spectra were recorded. The value of λ_{max} varied slightly between conjugates, from 535 to 540 nm. The experiments of spectrofluorometry with the MBP3_16 conjugates were performed at their λ_{max} value and at a total concentration $[B]_0 = 1.0$ μM. The titrations of the conjugates by the antigen were performed with ≥14 concentrations of MalE (Fig. S7). The deduced values of K_d varied between 80 and 690 nM, i.e. between 1.8 and 16 times the value for MBP3_16(wt). The values of $\Delta F_\infty/F_0$ varied between 0.46 and 5.8 (Table 3).

The ranking, according to s_r, of the five MBP3_16 conjugates that we studied in detail, was the following when their concentration was $[B]_0 \geq 0.16$ μM: Lys89 > Asn45 > Ala78 > Ser76 > Met43 (Fig. S8). The lower limits of detection varied widely as a function of $[B]_0$. Its value for the MBP3_16(K89ANBD) conjugate was equal to 4.3 nM for $[B]_0 = 1.0$ μM, i.e. the concentration at which we performed our experiments.

4. Discussion

We have developed a general approach to construct RF biosensors from the members of artificial families of AgBPs and validated this approach with the H4S Nanofitin and the MBP3_16 DARPin. The binding site for the antigen is constituted by a number of hypervariable (or randomized) residues, supported by a constant polypeptide backbone. The hypervariable residues form a connected set at the surface of the AgBP and only a subset of them is used to bind a given antigen. As a result, some hypervariable residues are located in the neighborhood of the antigen binding site without belonging to this site.

Comparison of the K_d values for H4S(wt) and its conjugates showed that conjugation of the fluorophore at positions Trp22, Leu31, Ile33, Asn40, Tyr42 and Asp44 strongly decreased the free energy of interaction ΔG between H4S and HEL ($\Delta\Delta G \geq 1.5$ kcal mol^{-1}, subset R1). Conjugation at positions Trp8, Val21, Lys24, Ala26 and Lys39 affected it more mildly ($0.5 \leq \Delta\Delta G \leq 1.2$ kcal mol^{-1}, subset R2). Conjugation at positions Phe7, Asn9, Lys28, Ser29 and Thr46 did not affect adversely the interaction ($\Delta\Delta G \leq 0.5$ kcal mol^{-1}, subset R3). These experiments suggested that the residues of subset R1, which form a continuous patch at the surface of H4S, belonged to the binding site for HEL; that the residues of R2 were at the periphery of the binding site; and that those of R3 were located outside of it (Fig. 3). The positions that gave the most sensitive conjugates belonged to subset R2 (Table 1).

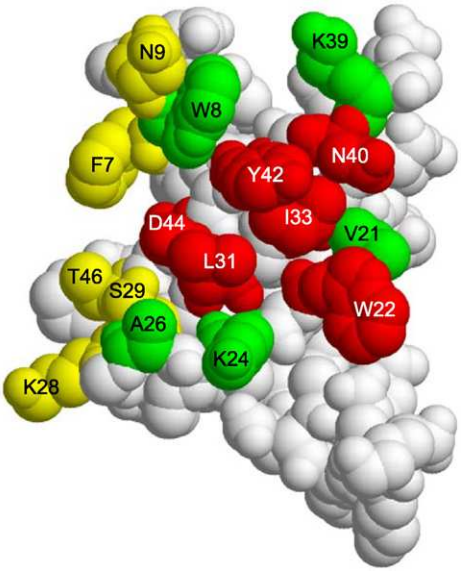

Fig. 3. Positions of the hypervariable positions in a structural model of H4S. The model was created with the Swiss Model program in the alignment mode and the crystal structure of the Sac7d protein at a resolution of 1.6 Å as a template (PDB: 1azp) (Arnold et al., 2006; Robinson et al., 1998). Red, positions where the coupling of the fluorophore strongly decreased the free energy of interaction between H4S and HEL ($\Delta\Delta G \geq 1.5$ kcal mol^{-1}); green, positions where the coupling mildly decreased the energy of interaction ($0.5 \leq \Delta\Delta G \leq 1.2$ kcal mol^{-1}) and resulted in the most sensitive conjugates; yellow, positions where the coupling did not decrease the interaction ($\Delta\Delta G \leq 0.5$ kcal mol^{-1}) and resulted in little sensitive or insensitive conjugates.

To identify the antigen binding site of MBP3_16, we changed the residues of its randomized positions individually into cysteine, and measured the K_d values between the corresponding mutant proteins and their MalE antigen. Six among the 12 mutations of the randomized positions decreased the interaction between MBP3_16 and MalE by $\Delta\Delta G > 1.1$ kcal mol^{-1}. These six residues form a tight cluster of residues at the surface of the canonical DARPin structure (Kohl et al., 2003). We obtained MBP3_16 conjugates with good sensitivities by targeting the hypervariable residues of MBP3_16 that were not important for the interaction with the antigen, as deduced from a Cys scanning, i.e. those that did not belong to the above cluster (Tables 2 and 3).

5. Conclusion

Thus, we showed that one can generate RF biosensors from artificial families of AgBPs by targeting, for the coupling of a fluorophore, the hypervariable positions that are little or not important for antigen binding. This approach is also valid for the natural family of antibodies, as shown retrospectively by our previous results (Renard et al., 2003). It could be applied to different types of fluorophores, e.g. ratiometric or working in the infra-red region of the

light spectrum. Moreover, by engineering the affinity of a conjugate through mutagenesis, it is possible to generate RF biosensors whose dynamic interval spreads over several orders of magnitude or, on the contrary, to generate derivatives whose affinity is abolished and which can be used as negative controls (Renard and Bedouelle, 2004). Reagentless fluorescent biosensors generated by this approach have numerous applications in health, environment, industrial processes, defense and fundamental research as they enable one to detect an antigen in a specific, selective, immediate and quantitative way, without any manipulation of the analyte sample or addition of reagent. The implementation of such biosensors could be done straightforwardly by using miniaturized low-cost optical devices.

Acknowledgements

We thank P. England and S. Hoos for their help with the Biacore instrument; and N. Guiso for her constant interest. Plasmids pQEMBP3_16, pQEMBP and pAT224 were gifts of A. Plückthun (University of Zürich). This work was supported by the Délégation Générale à l'Armement, Ministère de la Défense, France (DGA-REI 2008.34.0010 to H.B., DGA doctoral fellowship to E.B.-L.), Institut Pasteur (DARRI-2007 to H.B.), and La Région des Pays de Loire (to F.P.).

Appendix A. Supplementary data

Supplementary data associated with this article can be found, in the online version, at doi:10.1016/j.bios.2011.04.030.

References

Altschuh, D., Oncul, S., Demchenko, A.P., 2006. J. Mol. Recogn. 19, 459–477.
Arcus, V., 2002. Curr. Opin. Struct. Biol. 12, 794–801.
Arnold, K., Bordoli, L., Kopp, J., Schwede, T., 2006. Bioinformatics 22, 195–201.
Beste, G., Schmidt, F.S., Stibora, T., Skerra, A., 1999. Proc. Natl. Acad. Sci. U. S. A. 96, 1898–1903.
Binz, H.K., Amstutz, P., Kohl, A., Stumpp, M.T., Briand, C., Forrer, P., Grutter, M.G., Pluckthun, A., 2004. Nat. Biotechnol. 22, 575–582.
Binz, H.K., Stumpp, M.T., Forrer, P., Amstutz, P., Pluckthun, A., 2003. J. Mol. Biol. 332, 489–503.
Brient-Litzler, E., Pluckthun, A., Bedouelle, H., 2010. Protein Eng. Des. Sel. 23, 229–241.
Bullock, W.O., Fernandez, J.M., Short, J.M., 1987. Biotechniques 5, 376–379.
Cinier, M., Petit, M., Williams, M.N., Fabre, R.M., Pecorari, F., Talham, D.R., Bujoli, B., Tellier, C., 2009. Bioconjug. Chem. 20, 2270–2277.
Drevelle, A., Urvoas, A., Hamida-Rebai, M.B., Van Vooren, G., Nicaise, M., Valerio-Lepiniec, M., Desmadril, M., Robert, C.H., Minard, P., 2009. Chembiochem 10, 1349–1359.
Famm, K., Hansen, L., Christ, D., Winter, G., 2008. J. Mol. Biol. 376, 926–931.
Heyd, B., Pecorari, F., Collinet, B., Adjadj, E., Desmadril, M., Minard, P., 2003. Biochemistry 42, 5674–5683.
Jespers, L., Schon, O., Famm, K., Winter, G., 2004. Nat. Biotechnol. 22, 1161–1165.
Kohl, A., Binz, H.K., Forrer, P., Stumpp, M.T., Pluckthun, A., Grutter, M.G., 2003. Proc. Natl. Acad. Sci. U. S. A. 100, 1700–1705.
Li, J., Mahajan, A., Tsai, M.D., 2006. Biochemistry 45, 15168–15178.
Loving, G.S., Sainlos, M., Imperiali, B., 2010. Trends Biotechnol. 28, 73–83.
MacCallum, R.M., Martin, A.C., Thornton, J.M., 1996. J. Mol. Biol. 262, 732–745.
Mosavi, L.K., Cammett, T.J., Desrosiers, D.C., Peng, Z.Y., 2004. Protein Sci. 13, 1435–1448.
Mosavi, L.K., Minor Jr., D.L., Peng, Z.Y., 2002. Proc. Natl. Acad. Sci. U. S. A. 99, 16029–16034.
Mouratou, B., Schaeffer, F., Guilvout, I., Tello-Manigne, D., Pugsley, A.P., Alzari, P.M., Pecorari, F., 2007. Proc. Natl. Acad. Sci. U. S. A. 104, 17983–17988.
Nieba, L., Krebber, A., Pluckthun, A., 1996. Anal. Biochem. 234, 155–165.
Nord, K., Gunneriusson, E., Ringdahl, J., Stahl, S., Uhlen, M., Nygren, P.A., 1997. Nat. Biotechnol. 15, 772–777.
Pecorari, F., Alzari, P.M., 2008. Patent Publication Nos. EP2099817 (A2), WO2008068637 (A3); Date of Priority, 04/12/2006; Applicants: Institut Pasteur and CNRS.
Renard, M., Bedouelle, H., 2004. Biochemistry 43, 15453–15462.
Renard, M., Belkadi, L., Bedouelle, H., 2003. J. Mol. Biol. 326, 167–175.
Robinson, H., Gao, Y.G., McCrary, B.S., Edmondson, S.P., Shriver, J.W., Wang, A.H., 1998. Nature 392, 202–205.
Smith, P.A., Tripp, B.C., DiBlasio-Smith, E.A., Lu, Z., LaVallie, E.R., McCoy, J.M., 1998. Nucleic Acids Res. 26, 1414–1420.
Theobald, D.L., Mitton-Fry, R.M., Wuttke, D.S., 2003. Annu. Rev. Biophys. Biomol. Struct. 32, 115–133.
Urvoas, A., Guellouz, A., Valerio-Lepiniec, M., Graille, M., Durand, D., Desravines, D.C., van Tilbeurgh, H., Desmadril, M., Minard, P., 2010. J. Mol. Biol. 404, 307–327.
Vessman, J., Stefan, R.I., Van Staden, J.F., Danzer, K., Lindner, W., Burns, D.T., Fajgelj, A., Muller, H., 2001. Pure Appl. Chem. 73, 1381–1386.

Supplementary data for

Reagentless fluorescent biosensors from artificial families of antigen binding proteins

Frederico F. Miranda[a,b,1], Elodie Brient-Litzler[a,b,1], Nora Zidane[a,b], Frédéric Pecorari[c,d] and Hugues Bedouelle[a,b,*]

[a] Institut Pasteur, Department of Infection and Epidemiology, Unit of Molecular Prevention and Therapy of Human Diseases, 25 rue Docteur Roux, 75724 Paris Cedex 15, France.

[b] CNRS URA3012, 25 rue Docteur Roux, 75724 Paris Cedex 15, France.

[c] CNRS UMR6204, Biotechnology, Biocatalysis and Bioregulation, 2 rue de la Houssinière, BP 92208, 44322 Nantes Cedex 3, France.

[d] Université de Nantes, Faculté des Sciences et des Techniques, 2 rue de la Houssinière, BP 92208, 44322 Nantes Cedex 3, France.

* Corresponding author at: Institut Pasteur, CNRS URA3012, 25 rue Docteur Roux, 75724 Paris Cedex 15, France. Tel: +33 1 45688379; fax: +33 1 40613533.

Email address: hugues.bedouelle@pasteur.fr

[1] These authors contributed equally to this work.

S1. Supplementary materials and methods

Buffers

Buffer A was 500 mM NaCl, 50 mM Tris-HCl, pH 8.0; buffer B, as buffer A but pH 7.5; buffer C, 150 mM NaCl, 50 mM Tris-HCl, pH 7.4; buffer D, 0.005% (v/v) Tween 20, 0.1 mg/mL BSA in buffer C; buffer E, 5 mM dithiothreitol (DTT) in buffer D; buffer F, 0.005 % (v/v) Tween 20 and 5 mM DTT in buffer C. Phosphate buffered saline (PBS) was purchased from Sigma-Aldrich.

Mutagenesis of the MBP3_16 gene

DARPins are formed of repeated polypeptidic modules and encoded by repeated segments of DNA. These repetitions constitute a problem for the construction of mutations by site-directed mutagenesis. We used the degeneracy of the genetic code to design a mutant allele of the *mbp3_16* gene, that was devoid of important repetitions. The mutant allele, *mbp3_16-1,* was synthesized by Genecust (Evry, France) and inserted in the same plasmid vector pQE30 (Qiagen) as the parental gene, to give the recombinant plasmid pQEMBP3_16-1. Changes of residues were introduced in the MBP3_16 protein at the genetic level, by mutagenesis of either pQEMBP3_16 for A78C and D81C, or pQEMBP3_16-1 for the other mutations.

Protein production and purification

The parental protein H4S(wt) and its mutant derivatives were produced in the cytoplasm of the recombinant strain NEB-Express-I^q(pH4S) and its mutant derivatives as follows. The producing strains were grown at 30 °C. They were streaked on plates of LB agar, supplemented with ampicillin at 100 μg/mL and chloramphenicol at 10 μg/mL. A pre-culture in 2-YT broth, supplemented with the same two antibiotics, was inoculated with an isolated colony and grown overnight. A larger culture (650 mL), supplemented with ampicillin alone, was inoculated with an aliquot of the preculture to obtain a starting absorbance A_{600nm} = 0.1, grown until A_{600nm} = 0.8, induced with 1 mM IPTG, and then grown further for 24 hours. The following purification steps were performed at 4 °C. The culture was chilled on ice,

centrifuged at 8000*g* for 20 min and the resulting pellet was frozen and kept at -20 °C. The pellet was resuspended in 30 ml of 5 mM imidazole in buffer A and the cells were disintegrated by sonication. The lysate was centrifuged at 8600*g* for 30 min and the supernatant filtered through a 0.22 μm Millex filter (Millipore). H4S(wt) and its derivatives were purified from the corresponding lysate through their hexahistidine tag by affinity chromatography on a column of Ni-NTA resin. The protein was eluted from the resin with 200 mM imidazole in buffer A.

Fluorophore coupling

The conjugates between the cysteine mutants of the antigen binding protein (AgBP) and the thiol reactive fluorophore IANBD ester were prepared essentially as described (Brient-Litzler et al., 2010). Briefly, the AgBP mutants were reduced with 5 mM DTT for 30 min at 30 °C with gentle shaking and then the buffer was exchanged to PBS by size exclusion chromatography with a PD10 column (GE Healthcare). From this point on, all the experiments were done in the dark. The IANBD ester was added in a 10:1 molar excess over the AgBP mutant and the coupling reaction was carried out for 2.5 hours at 30 °C with gentle shaking. The denatured proteins were removed by centrifugation for 30 min at 13200*g*, 4 °C. The conjugate was separated from the unreacted fluorophore by chromatography on a Ni-NTA column (0.5 mL of resin) and eluted with imidazole in buffer A for the H4S derivatives or buffer B for the MBP3_16 derivatives. The conjugate between 2-mercaptoethanol and the IANBD ester was prepared by mixing the two molecules in stoechiometric amounts and then incubating the mixture for 30 min at 25 °C. The coupling yield y_c, i.e. the average number of fluorophore molecule coupled to each AgBP molecule, was calculated as described below, with ε_{280}(ANBD) = 2100 M^{-1} cm^{-1}, ε_{500}(ANBD) = 31800 M^{-1} cm^{-1}, both measured with conjugates between IANBD and 2-mercaptoethanol (Renard et al., 2002).

Let P be a protein; B, a monoconjugate between P and IANBD; Φ, the conjugated form of IANBD; A_{280} and A_{500}, the absorbances of the mixture of P and B that results from the coupling reaction and elimination of the unconjugated fluorophore. By definition,

$$y_c = [B]/([B] + [P]) \quad \text{(S1)}$$

where [B] and [P] are concentrations. Then, the reciprocal of the coupling yield is given by the following equation where ε is a molar absorbance (Brient-Litzler et al., 2010):

$$y_c^{-1} = (A_{280}/\varepsilon_{280}(P))(A_{500}/\varepsilon_{500}(\Phi))^{-1} - \varepsilon_{280}(\Phi)/\varepsilon_{280}(P) \quad \text{(S2)}$$

Interaction between AgBP and antigen

A conjugate (or biosensor) B and antigen A form a 1:1 complex B:A according to the reaction:

$$B + A \leftrightarrow B{:}A \quad \text{(S3)}$$

At equilibrium, the concentration [B:A] of the complex is given by the equation:

$$[B{:}A] = 0.5\{[B]_0 + [A]_0 + K_d - (([B]_0 + [A]_0 + K_d)^2 - 4\,[B]_0[A]_0)^{1/2}\} \quad \text{(S4)}$$

where K_d is the dissociation constant, and $[A]_0$ and $[B]_0$ are the total concentrations of A and B, respectively (Renard et al., 2003).

Quenching by potassium iodide

The experiments of fluorescence quenching by KI were performed at 25 °C in Buffer C, essentially as described for the titration experiments. The Stern-Volmer Eq. (S5) was fitted to the experimental data, where F and F^0 are the intensities of fluorescence for the AgBP conjugate in the presence or absence of quencher, respectively. The Stern-Volmer constant K_{SV} was used as a fitting parameter.

$$F^0/F = 1 + K_{SV}\,[KI] \quad \text{(S5)}$$

Affinity in solution as determined by competition Biacore

The binding reactions (250 µl) between the H4S Nanofitin and its HEL antigen were conducted by incubating 20 nM of H4S with variable concentrations of HEL for 30 min in buffer D. The concentration of free H4S was then measured by surface plasmon resonance with a Biacore 2000 instrument (Biacore Life Sciences). Lysozyme was immobilized (700 Resonance Units, RU) on the surface of a CM5 sensor chip (Biacore Life Sciences) and the reaction mixtures were injected in the sensor chip at a flow rate of 30 µL min^{-1}. The chip surface was regenerated between the runs by injecting 10 µL of a 0.05% SDS solution.

The binding reactions (100 µL) between the MBP3_16 DARPin and its MalE antigen were conducted by incubating a fixed concentration of MBP3_16 molecules with variable concentrations of MalE for > 1 h in buffer F. The wild type MBP3_16(wt) and its mutant derivatives were used at a concentration of 50 nM, except those carrying mutations T79C, D81C and W90C, which were used at 500 nM to obtain a sufficient signal. A high density (> 2000 RU) of the biotinylated form of MalE (bt-MalE) was immobilized on the surface of a streptavidin SA sensorchip (Biacore Life Sciences). Each reaction mixture was injected in the sensor chip at a flow rate of 25 µL min^{-1}. The chip surface was regenerated by injecting 10 µL of a glycine-HCl solution at pH 3.0 (Biacore Life Sciences) between each run.

The following equation results from the laws of mass action and conservation:

$$[P] = 0.5\{[P]_0 - [A]_0 - K_d + (([P]_0 - [A]_0 - K_d)^2 + 4\,K_d[P]_0)^{1/2}\} \quad \text{(S6)}$$

where $[A]_0$ is the total concentration of antigen in the reaction mixture; $[P]_0$, the total concentration of AgBP; and [P], the concentration of free AgBP (Lisova et al., 2007). The association between the reaction mixture at equilibrium and immobilized antigen was monitored as described (Brient-Litzler et al., 2010). In these conditions, the initial slope r of the association curve follows the equation:

$$r = r_0[P]/[P]_0 \quad \text{(S7)}$$

where r_0 is the value of r for $[A]_0 = 0$. The values of K_d and r_0 were determined by fitting Eq. (S7), in which [P] is given by Eq. (S6), to the experimental values of r.

Kinetic measurements by Biacore

The kinetics were measured in buffer E at a flow rate of 30 µL min^{-1} with CM5 sensor chips. A first cell of the sensor chip was used as a reference, i.e. no ligand was immobilized on the corresponding surface. A second cell was loaded with 500-1000 RU of HEL. Solutions (200 µL) of the H4S derivatives at 15 different concentrations (1 nM to 6 µM) were injected to monitor association and then buffer alone (150 µL) for dissociation. The chip surface was regenerated between the runs by injecting 10 µL of a 0.05% SDS solution. The signal of the buffer alone was subtracted from the raw signals to obtain the protein signals, and then the protein signal on cell 1 was subtracted from the protein signal on cell 2 to obtain the specific

signal of interaction. The kinetic data were cleaned up with the Scrubber program (Biologic Software) and then the kinetic parameters were calculated by applying a simple model of Langmuir binding and a procedure of global fitting, as implemented in the Bia-evaluation 4.1 software (Biacore Life Sciences).

Data analysis

The fittings of equations to experimental data were performed with the Kaleidagraph software (Synergy Software). The standard error (SE) on the free energy of dissociation $\Delta G = -RT\ln K_d$ was deduced from the SE value on K_d by the equation:

$$SE(\Delta G) = RT SE(K_d)/K_d \quad \text{(S8)}$$

The SE value on the variation of interaction energy resulting from a mutation $\Delta\Delta G = \Delta G(\text{wt}) - \Delta G(\text{mut})$ was deduced from the SE values on ΔG by the equation:

$$[SE(\Delta\Delta G)]^2 = [SE(\Delta G(\text{wt}))]^2 + [SE(\Delta G(\text{mut}))]^2 \quad \text{(S9)}$$

S2. Supplementary Results

Binding parameters of H4S derivatives

The K_d values of the H4S conjugates varied with the position of the fluorophore (Table 1). To determine whether these variations in affinity were due to the mutation of the parental side chain into Cys or to the coupling of the fluorescent group, we measured the kinetic parameters of interaction between H4S(wt) and five of its cysteine mutants on the one hand, and hen egg white lysozyme (HEL) on the other hand by Biacore (Section S1). The kinetics were measured in the presence of dithiothreitol to prevent dimerization of the cysteine mutants. We analyzed the kinetic data with a 1:1 model, calculated the corresponding dissociation constant from the rate constants, i.e. $K_d' = k_{off}/k_{on}$, and also derived the dissociation constant at steady state K_d'' from these kinetic experiments (Table S1). We found that the values of K_d, K_d' and K_d'' were close for H4S(wt), 40 ± 2 nM, 31 nM and 18 nM respectively. The K_d value, determined in solution, was slightly higher than the K_d' and K_d'' values, determined at the interface between a solid and a liquid phase. Comparison of the K_d, K_d' and K_d'' values between H4S(wt) and either the Cys mutants or the conjugates indicated that the lower affinity of the conjugates relative to H4S(wt) was mainly due to the mutation into Cys at positions Val21 and Lys24, whereas it was mainly due to the coupling of the fluorophore at positions Trp8, Ala26 and Lys39.

Mechanism of fluorescence variation

Eleven of the H4S conjugates were sensitive to the binding of HEL, with $\Delta F_\infty/F_0$ between 0.5 and 8.8. We used potassium iodide (KI) to explore the physico-chemical mechanism by which the fluorescence intensity of the conjugates varied on antigen binding. We found that the fluorescence of the H4S(K24ANBD) conjugate was quenched by KI, both in its free and HEL-bound states. The quenching varied linearly with the concentration of KI (Fig. S4). This law of variation indicated that the molecules of fluorophore were identically exposed to KI and constituted a homogeneous population in either case (Lakowicz, 1999). It confirmed that the fluorescent group was specifically coupled to the mutant cysteine. The Stern-Volmer

constant was higher for the free conjugate than for its complex with the target antigen: K_{SV} = 6.7 ± 0.1 M^{-1} versus 2.5 ± 0.1 M^{-1} (SE in the curve fits of Fig. S4). These values indicated a lower accessibility of the fluorophore to KI in the bound state of the conjugate than in its free state. They showed that the fluorescence increase was due to a shielding of the fluorescent group from the solvent by the binding of the antigen, as previously observed for other conjugates with IANBD (Renard et al., 2003; Brient-Litzler et al., 2010). Thus the mechanism of fluorescence variation was consistent with our rules of design.

Fluorescence variation in serum

We observed that the fluorescence response of the H4S(K24ANBD) conjugate was lower in serum than in buffer, as reported previously for conjugates between IANBD and other proteins (Renard et al., 2003; Brient-Litzler et al., 2010). To better understand this difference, we measured the variations of the F_0 and F_∞ parameters as functions of the concentration in serum. We used a conjugate between IANBD and 2-mercaptoethanol as a control (Fig. S3). The absorbance of the serum alone increased linearly with its concentration, in agreement with the Beer-Lambert law, at both 485 nm and 536 nm, which were the wavelengths of fluorescence excitation and emission in our experiments. The value of F_∞ for H4S(K24ANBD) decreased linearly with the concentration in serum. Therefore, the absorption of the excitation and emission lights by serum could account for the variation of F_∞. The value of F_0 for H4S(K24ANBD) increased with the concentration in serum, up to 35% (v/v) of serum, and then decreased slowly. We observed the same variations for the conjugate between IANBD and 2-mercaptoethanol. Therefore, the initial increase of F_0 could result from the interaction between the fluorescent group and molecules of the serum, until saturation, and its subsequent decrease from the absorbance of light by the serum.

Supplementary references

Binz, H.K., Amstutz, P., Kohl, A., Stumpp, M.T., Briand, C., Forrer, P., Grutter, M.G., Pluckthun, A., 2004. High-affinity binders selected from designed ankyrin repeat protein libraries. Nat. Biotechnol. 22, 575-582.

Brient-Litzler, E., Pluckthun, A., Bedouelle, H., 2010. Knowledge-based design of reagentless fluorescent biosensors from a designed ankyrin repeat protein. Protein Eng. Des. Sel. 23, 229-241.

Lakowicz, J.R., 1999. Principles of fluorescent spectroscopy, 2nd ed. Kluwer Academic/Plenum, New York.

Lisova, O., Hardy, F., Petit, V., Bedouelle, H., 2007. Mapping to completeness and transplantation of a group-specific, discontinuous, neutralizing epitope in the envelope protein of dengue virus. J. Gen. Virol. 88, 2387-2397.

Renard, M., Belkadi, L., Bedouelle, H., 2003. Deriving topological constraints from functional data for the design of reagentless fluorescent immunosensors. J. Mol. Biol. 326, 167-175.

Renard, M., Belkadi, L., Hugo, N., England, P., Altschuh, D., Bedouelle, H., 2002. Knowledge-based design of reagentless fluorescent biosensors from recombinant antibodies. J. Mol. Biol. 318, 429-442.

Legends to the supplementary figures

Fig. S1. Sequence of the parental H4S Nanofitin. The numbering does not take the first 11 residues into account. The randomized positions are colored red; residues Lys28 and Lys39 are colored green.

Fig. S2. Sequence of the parental MBP3_16 DARPin. AR1 and AR2, ankyrin repeats 1 and 2 respectively. Positions 2, 3, 5, 13, 14, and 33 in each ankyrin repeat are fully randomized and colored red. Position 26 in each repeat is partially randomized and colored green. Position 43 in the N-cap module is fully randomized and position 109 in AR2 is not randomized (Binz et al., 2004).

Fig. S3. Effect of the concentration in serum on the fluorescence signal for conjugates between IANBD and either H4S(K24C) or 2-mercaptoethanol. The experiments were performed in a mixture (v:1-v) of serum and buffer C at 25 °C. The total concentration of conjugate was equal to 0.3 μM. The total concentration of HEL was equal to 10 μM and thus saturating (see Table 1). Open squares, 2-mercaptoethanol-ANBD (the results were identical in the presence or absence of HEL); open circles, H4S(K24ANBD) without HEL; closed circles, H4S(K24ANBD) with HEL. *F*, intensity of fluorescence in arbitrary units. The continuous curves were drawn only for clarity.

Fig. S4. Quenching of the H4S(K24ANBD) fluorescence by KI. *F* and F^0, fluorescence of the conjugate with and without quencher respectively. The experiments were performed in buffer C at 25 °C. The concentration of conjugate was equal to 0.3 μM. The continuous curves were obtained by fitting Eq. (S5) to the experimental data. Closed circles, conjugate in the absence of HEL; open circle, conjugate in the presence of a saturating concentration of HEL (10 μM). The corresponding Stern-Volmer constants K_{SV} were equal to 6.7 ± 0.1 M^{-1} and 2.5 ± 0.1 M^{-1} respectively (value ± SE in the fitting).

Fig. S5. Determination of the dissociation constant K_d between MBP3_16(wt) and MalE in solution at 25 °C in buffer F, by competition Biacore. The total concentration of MalE in the binding reaction is given along the *x* axis. The *r* signal, which is proportional to the concentration of free MBP3_16(wt) in the binding reaction, is given along the *y* axis. Fifteen concentrations of MalE were used. The curve was obtained by fitting Eq. (S7) to the experimental data, with K_d and r_0 as floating parameters.

Fig. S6. Relation between R_{eq} and K_d for the interaction between MalE and the Cys mutants of MBP3_16. The values of R_{eq} and K_d were determined by Biacore (Table 2). The curve was obtained by fitting Eq. (8) to the experimental values of R_{eq} and K_d, with C = [MBP3_16] = 50 nM and R_{max} as a floating parameter. The values of R_{max} and Pearson coefficient R in the fitting were equal to 595 ± 27 RU and 0.96524 respectively.

Fig. S7. Titration of MBP3_16 conjugates by MalE, monitored by fluorescence. The experiments were performed at 25 °C in buffer C. The total concentration in MBP3_16, as measured by A_{280nm}, was equal to 1.0 μM. The total concentration in MalE protein is given along the *x* axis; a data point at 10 μM is not shown on the figure. The continuous curves correspond to the fitting of Eq. (2) to the experimental values of $\Delta F/F_0$ (Section 2.3). Open triangle, position Met43; open circle, Asn45; closed triangle, Ala78; closed circle, Lys89.

Fig. S8. Relative sensitivities s_r of MBP3_16 conjugates at 25 °C in buffer C as a function of their concentration. This figure is a plot of Eq. (5), using the parameters listed in Table 3. Open triangle, position Met43; open circle, Asn45; closed triangle, Ala78; closed circle, Lys89. The curve for Ser76 has not been represented for clarity; it is located between those for Met43 and Ala78.

Table S1. Binding parameters for the Cys mutants of H4S, as determined by Biacore experiments.

Mutation	Monomer (%)	k_{on} (10^5 M^{-1} s^{-1})	k_{off} (10^{-2} s^{-1})	K_d' (nM)	K_d" (nM)
WT	100	4.9	1.5	31	18
W8C	86	4.5	3.0	68	66
V21C	88	0.4	1.1	332	389
K24C	100	1.6	2.3	117	104
A26C	80	3.8	2.3	60	54
K39C	85	3.1	1.2	38	24

WT, parental H4S protein. The percentage of monomers was quantified with the Un-scan-it software (Silk Scientific), as described in Section 2.2. HEL was immobilized on a CM5 sensorchip. The association and dissociation rate constants, k_{on} and k_{off}, were determined at 25 °C in buffer E and used to calculate $K_d' = k_{off}/k_{on}$. K_d" is the dissociation constant at steady state. We applied a simple kinetic model of Langmuir binding (Section S1).

H4S

```
-10          1         10         20         30
 MRGSHHHHHHGSVKVKFFWNGEEKEVDTSKIVWVKRAGKSV
           40         50         60
  LFIYDDNGKNGYGDVTEKDAPKELLDMLARAEREKKLN
```

Figure S1

MBP3_16

```
       1        10         20         30         40
N-cap: MRGSHHHHHHGSDLGKKLLEAAHAGQDDEVRILMANGADVNAM
                      50         60         70
AR1   :             DNFGVTPLHLAAYWGHFEIVEVLLKYGADVNAS
                      80         90        100
AR2   :             DATGDTPLHLAAKWGYLGIVEVLLKYGADVNAQ
                   110        120        130
C-cap:              DKFGKTAFDISIDNGNEDLAEILQKLN
```

Figure S2

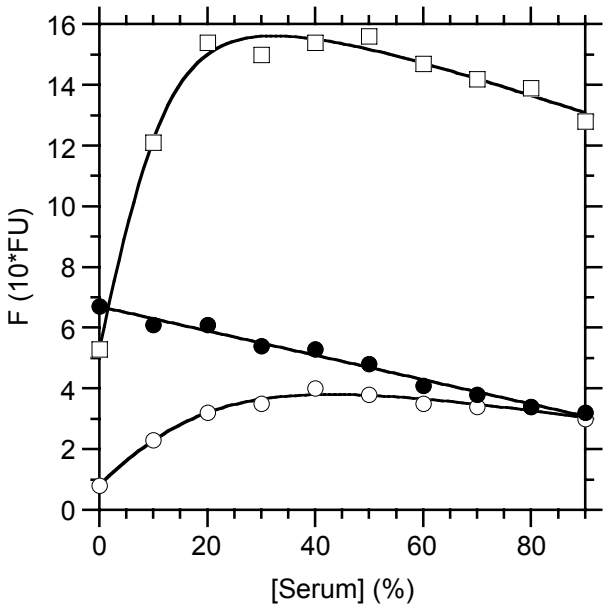

Figure S3

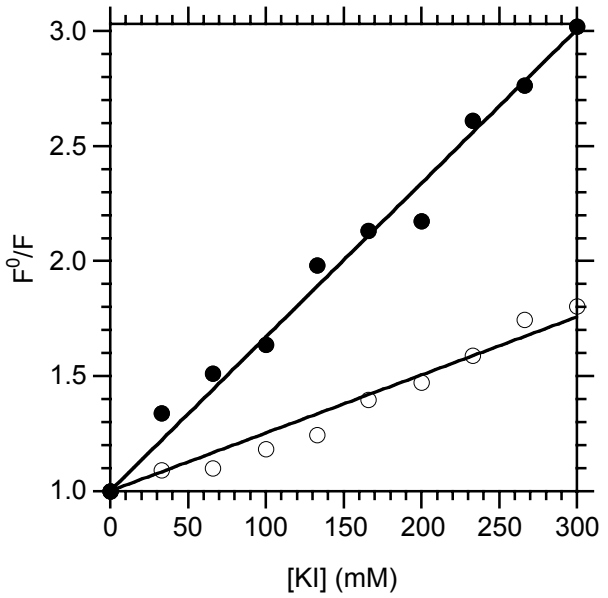

Figure S4

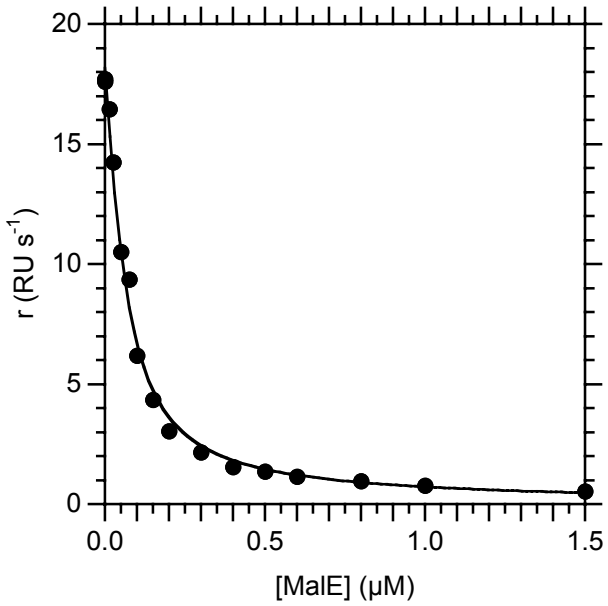

Figure S5

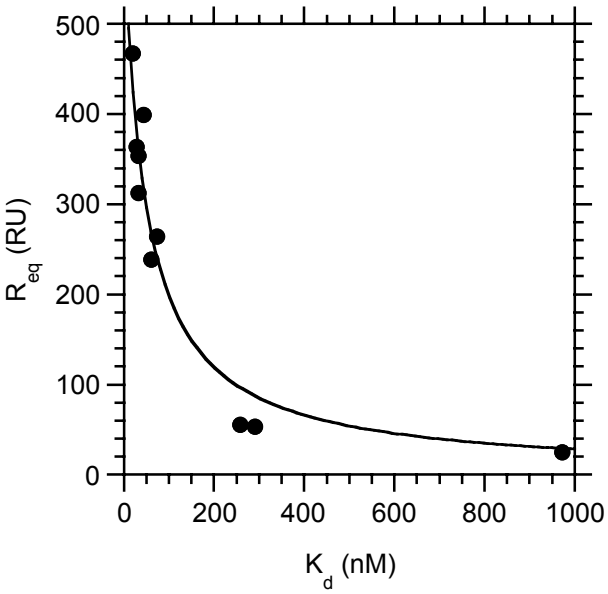

Figure S6

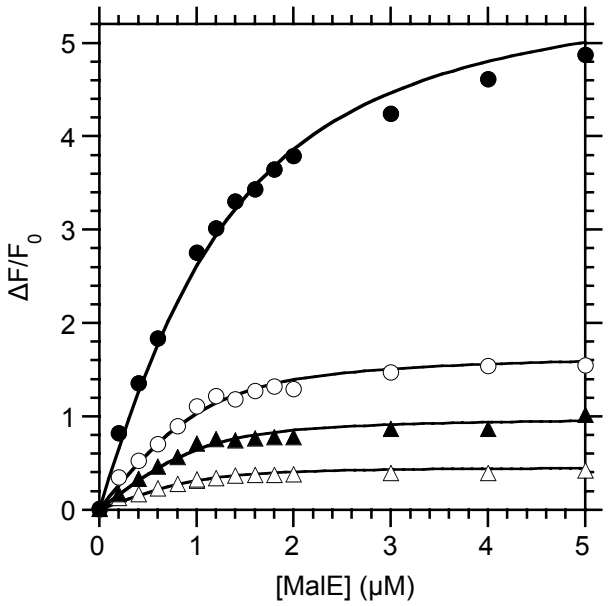

Figure S7

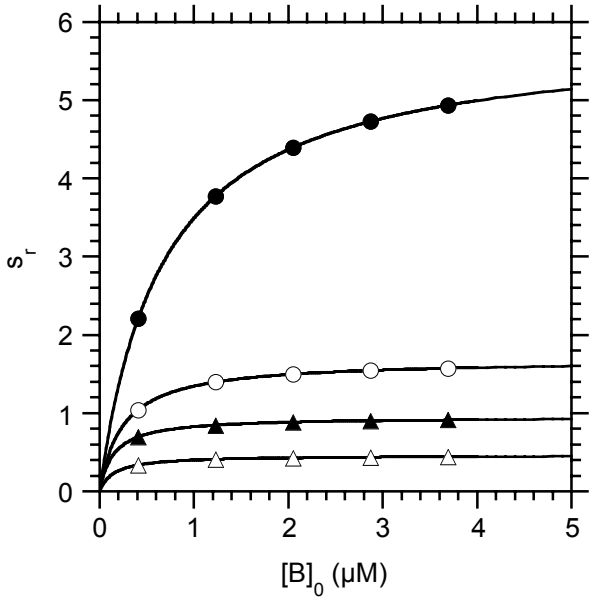

Figure S8